Microchimica Acta (2022) 189: 49
https://doi.org/10.1007/s00604-021-05141-0

ORIGINAL PAPER

Sandwich-type microRNA biosensor based on graphene oxide incorporated 3D-flower-like MoS_2 and AuNPs coupling with HRP enzyme signal amplification

Jiangbo Dong[1] · Huisi Yang[1] · Jiaying Zhao[1] · Li Wen[1] · Congjuan He[1] · Zhikun Hu[1] · Jiawei Li[2,3] · Danqun Huo[1,3] · Changjun Hou[1,4]

Received: 17 September 2021 / Accepted: 8 December 2021 / Published online: 6 January 2022

Abstract

A sandwich electrochemical biosensing strategy for ultrasensitive detection of miRNA-21 was developed by using graphene oxide incorporated 3D-flower-like MoS_2 (3D MoS_2-rGO) nanocomposites as the substrate and horseradish peroxidase (HRP)-functionalized DNA strand 1 (S1)-gold nanoparticles (S1-AuNPs-HRP) as signal amplification probes. Herein, 3D MoS_2-rGO nanocomposites not only had a large specific surface area and excellent conductivity, but also provided more attachment sites for electrodepositing AuNPs. In the presence of target miRNA, a sandwich structure was formed, and the determination of the miRNA-21 was carried out by measuring the DPV response of H_2O_2 mediated by hydroquinone (HQ) at a potential of + 0.052 V (vs AgCl reference electrode). Under the optimal experimental conditions, the as-prepared biosensor enabled the ultrasensitive detection of miRNA-21 from 5 fM to 0.5 μM with the low detection limit of 0.54 fM ($S/N = 3$), comparable or lower than previous reported methods for miRNA-21 detection, which benefited from the synergistic amplification of 3D MoS_2-rGO and AuNPs-HRP. The prepared biosensor showed satisfactory selectivity, reproducibility, and stability towards miRNA-21 detection. The biosensor was feasible for accurate and quantitative detection of miRNA-21 in normal human serum samples with RSD below 5.86%, which showed a great potential in clinical analysis and disease diagnosis.

Keywords Sandwich structure · MoS_2 · Electrochemical biosensor · Differential pulse voltammetry · AuNPs · Synergistic amplification · miRNA-21

✉ Jiawei Li
LI_JIAWEI_1993@163.com

✉ Danqun Huo
huodq23@163.com

✉ Changjun Hou
houcj@cqu.edu.cn

[1] Key Laboratory for Biorheological Science and Technology of Ministry of Education, State and Local Joint Engineering Laboratory for Vascular Implants, Bioengineering College of Chongqing University, Chongqing 400044, People's Republic of China

[2] Chongqing University Three Gorges Hospital, Chongqing 404000, People's Republic of China

[3] Chongqing Key Laboratory of Bio-Perception & Intelligent Information Processing, School of Microelectronics and Communication Engineering, Chongqing University, Chongqing 400044, People's Republic of China

[4] National Facility for Translational Medicine (Shanghai), Shanghai 200240, People's Republic of China

Introduction

MicroRNAs (miRNAs), a kind of noncoding single-stranded RNA molecule with a length of 19–25 nucleotides, have an important effect in biological processes, such as tissue differentiation, growth control, and apoptosis [1–3]. Recent accumulative studies have shown that the abnormal expression of microRNAs may be associated with cancer, genetic diseases, heart disease, AIDS, neurological diseases, obesity, etc. [4–6]. Thus, the determination of concentration of miRNAs in biological samples has far-reaching significance in diagnostic studies. Up to now, varieties of analytical technologies have been developed to detect miRNAs including real-time quantitative PCR (qPCR) [7], Northern blotting [8], and fluorescent assay [9]. However, these conventional techniques are limited by complicated operation, high cost, and sample-consuming. To address these challenges, some methods have been extended to the manufacture of biosensors to detect

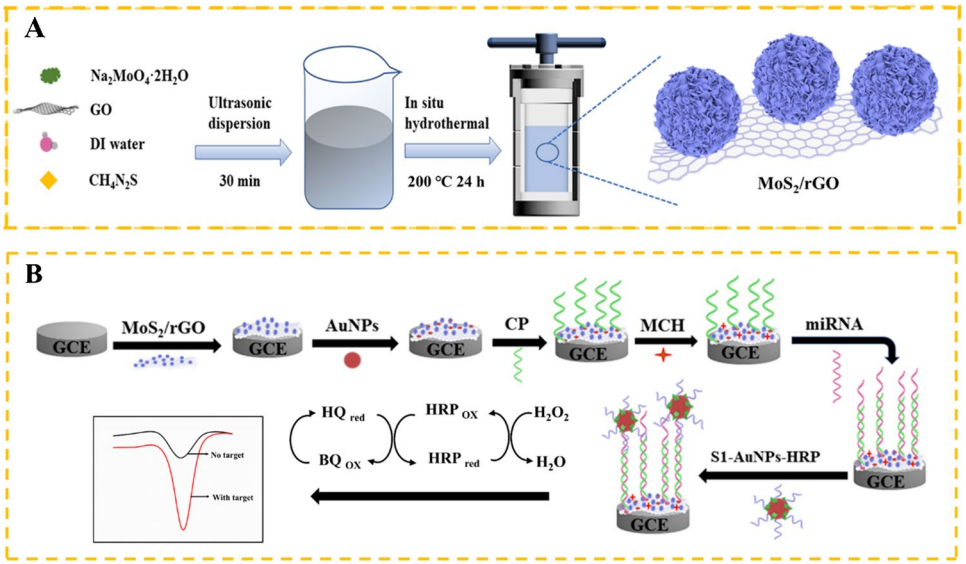

Scheme 1 **A** Preparation process for MoS_2-rGO. **B** Schematic diagram of miRNA-21 detection based on MoS_2-rGO and HRP strategy

miRNAs, including electrochemical assay [10], electrochemiluminescence [11], microfluidic technology [12], etc. Among them, electrochemical sensors have attracted much attention in biomarker detection due to their low cost, high specificity, simple operation, and miniaturization [13–16].

In order to achieve the high sensitivity of electrochemical biosensors, the surface fabrication of electrodes is an important component that needs to be improved. The application of two-dimensional (2D) layered nanomaterials [17–20], such as MoS_2, provides a strategy for enhancing the performance of electrochemical biosensors. MoS_2 is an analogous nanomaterial to GO, with a S-Mo-S layered skeleton, giving it a unique electronic structure, which is beneficial to improve detection sensitivity [21]. However, MoS_2 is easy to overlap and aggregate owing to the strong van der Waals between S-Mo-S layers, which would seriously affect the performance of MoS_2 as an electrode modification material [22]. To solve the above problem, a common method is to hybridize MoS_2 with other nanomaterials, such as carbon dots, graphene oxide (GO), and CNT [23], in which graphene is the preferred hybrid material due to its abundant functional groups [24–26]. In addition to substrate materials, the preparation of various nanoprobes loaded with different signal labels has also received significant attention and is widely applied in signal transduction of biosensors [27]. Among multiple nanoprobes, HRP-functionalized Au NPs nanoprobes have been employed for the signal amplification of different electrochemical biosensors due to their good biocompatibility, high catalytic activity, and long-term stability [28, 29].

So far, numerous efforts have been reported on the MoS_2, rGO, and HRP for the electrochemical detection of miRNAs [30–32]. However, to the best of our knowledge, there are few reports exploring the combination of MoS_2, rGO, and HRP-functionalized gold nanoprobes for miRNA detection and analysis. Herein, we constructed a sandwich-type biosensor platform based on MoS_2-rGO nanocomposites as the modified electrode's substrate and AuNPs-HRP as signal amplification nanoprobes for ultrasensitive and highly specific miRNA-21 detection (Scheme 1). Firstly, we synthesized the graphene oxide incorporated flower-like MoS_2 nanocomposites through one-step hydrothermal strategy and used them as electrode modification. The MoS_2-rGO exhibited a high specific surface area, unique three-dimensional structure, and uniform dispersion, which could load more AuNPs deposited by the electrochemical procedure to fix more capture probes and enhance the electron transport. Then, the thiolated capture probes were introduced onto the AuNPs/MoS_2-rGO surface via the Au–S bond. When the target miRNA-21 existed, S1-AuNPs-HRP, the bioconjugate functionalized signal nanoprobes, were linked to the modified electrode to form a sandwich-type structure. Finally, the signal amplification could be achieved by the synergistic amplification of 3D MoS_2-rGO and AuNPs-HRP in hydroquinone (HQ) and hydrogen peroxide (H_2O_2) system. This method showed high sensitivity and ideal selection to detect miRNA-21, and provided a universal and potential platform for ultrasensitive detection of clinically related diseases.

Experimental

The preparation of MoS_2-rGO and S1-AuNPs-HRP nanoprobes

The MoS_2-rGO was synthesized by one-step hydrothermal method [33], and S1-AuNPs-HRP nanoprobes were prepared following a previously published procedure with

slight modification [34]. The details were provided in the Electronic Supplementary Material.

PAGE gel electrophoresis

The PAGE gel electrophoresis analysis was performed on 20% polyacrylamide gel and ran at a constant voltage at 120 V for 90 min in 1 × TBE buffer (89 mM Tris, 89 mM boric acid, 2 mM EDTA, pH 8.3). The gel image was obtained using Azure Biosystems C150.

Fabrication of the modified electrodes

Firstly, the bare GCE was polished with 0.3 and 0.05 μm alumina powder, followed by sonicating in ethanol and deionized water. After being dried under N_2, 5 μL MoS_2-rGO suspension (0.5 mg mL^{-1}) was directly cast onto the surface of the GCE to obtain MoS_2-rGO/GCE. Then, the electrode was placed in 2 mM $HAuCl_4$ solution and electrodeposited at − 0.2 V for 120 s to obtain AuNPs/MoS_2-rGO/GCE. After that, 5 μL of 0.6 μM capture probes (CP) was cast onto the AuNPs/MoS_2-rGO/GCE and hybridized for 120 min at 37 °C to obtain CP/AuNPs/MoS_2-rGO/GCE. After washing with 100 mM PBS, 4 μL of 1 mM MCH was modified on the CP/AuNPs/MoS_2-rGO/GCE and hybridized for 30 min at 37 °C to block the unbound site to get MCH/CP/AuNPs/MoS_2-rGO/GCE. Finally, 5 μL of different concentrations of the miRNA-21 and 5 μL of S1-AuNPs-HRP conjugates were applied to the modified electrode, respectively, and incubated for 2 h at 37 °C, respectively, to obtain miRNA-21/MCH/CP/AuNPs/MoS_2-rGO/GCE and S1-AuNPs-HRP/miRNA-21/MCH/CP/AuNPs/MoS_2-rGO/GCE.

miRNA-21 detection in normal human serum

The detection of miRNA-21 in normal human serum was performed by the standard addition method. Firstly, the normal human serum was a commercial synthetic sample, which was purchased from Beijing Solarbio Technology Co., Ltd. Before the recovery experiments, the normal human serum was diluted tenfold by 0.01 M (pH = 7.4) PBS. Then, different concentrations of miRNA-21 (5 pM, 50 pM, 500 pM) were added to the diluted normal human serum. Following that, 5μL of the abovementioned diluted serum containing miRNA-21 of different concentrations was dropped onto the electrodes and incubated for subsequent experimental analysis. Thereafter, differential pulse voltammetry (DPV) was carried out to detect the concentration of miRNA-21 in spiked serum samples and recorded the current response value at a potential of 0.052 V. The DPV signal was finally converted to the molar concentration of miRNA-21 by comparing with the standard linear calibration curve to calculate the recovery.

Electrochemical measurements

Cyclic voltammetry (CV) and electrochemical impedance spectroscopy (EIS) were tested in 5 mM $[Fe(CN)_6]^{3-/4-}$ solution containing 0.1 M KCl. DPV was carried out in 5 mL PBS (100 mM, pH = 7.4) containing 2 mM H_2O_2 and 2 mM HQ, its parameter setting: the potential window was − 0.3 to 0.3 V, and the pulse amplitude was 0.05 V.

Results and discussion

Characterization of materials

The microstructures of MoS_2 and MoS_2/rGO were characterized by SEM. As shown in Fig. 1A and B, a mass of 2D MoS_2 were self-interconnected and assembled into a highly aggregated nanostructure [35]. After the introduction of rGO, as can be seen from Fig. 1C, D, and E, MoS_2 nanosheets were anchored on the surfaces of flake rGO via an in situ growth process, which was beneficial to prevent the accumulation of MoS_2 nanosheets and produced hybrid materials with a larger specific surface area. The rGO-MoS_2 nanocomposites with three-dimensional (3D) nanostructures, on the one hand, provided more loading sites for gold nanoparticles, and on the other hand also improved the sensitivity of the biosensor. EDS revealed that the elements of O, C, Mo, and S were evenly distributed on the surface of MoS_2/rGO (Fig. 1F). Additionally, XPS and XRD analyses of different nanomaterials are shown in Electronic Supplementary Material (Figs. S1 and S2). All these data above strongly validated the successful preparation of rGO-MoS_2.

The morphologies of AuNPs, S1-AuNPs, and S1-AuNPs-HRP were characterized by TEM (Fig. S3 A, B, and C). UV–Vis spectroscopy was applied to analyze and characterize S1-AuNPs-HRP probes (Fig. S3 D). The details are provided in the Electronic Supplementary Material.

Electrochemical study of MoS_2-rGO/GCE

To prove the feasibility of MoS_2-rGO/GCE in application of miRNA-21 detection, the electrochemical technology was adopted to study MoS_2-rGO/GCE. As displayed in Fig. 2A, CVs of different modified electrodes were performed on electrochemical workstation, respectively, and the results demonstrated that the nanocomposites had the excellent conductivity. Moreover, we calculated the electroactive surface area (A) by the Randles–Sevcik equation.

$$I_P = 2.69 \times 10^5 \times n^{3/2} A D^{1/2} v^{1/2} C \quad (1)$$

where I_p is the peak current (A); $n = 1$ (number of electronic transfers); $D = 6.7 \times 10^{-6}$ $cm^2 \cdot s^{-1}$

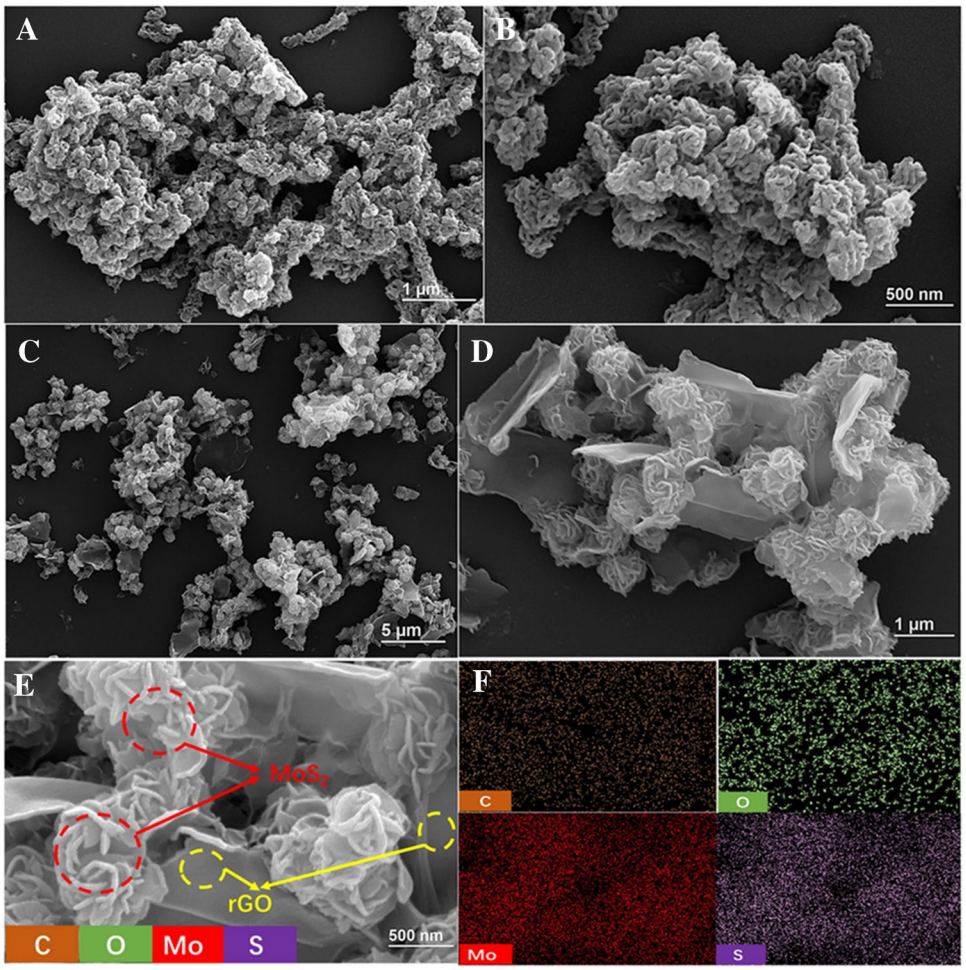

Fig. 1 SEM images of (**A**, **B**) MoS_2 and (**C**, **D**, **E**) MoS_2/rGO, and the corresponding EDS elemental mapping data (**F**) of MoS_2/rGO (**E**)

(diffusion coefficient); ν is the scan rate (V s^{-1}); and $C = 5 \times 10^{-6}$ mol·cm^3 (the concentration of the $[Fe(CN)_6]^{3-/4-}$). According to Eq. (1), the electroactive surface area of MoS_2-rGO/GCE was 0.0871 cm^2, which was about 1.22 times of bare GCE (0.0713 cm^2).

As displayed in Fig. 2B, a different scan rate was performed on MoS_2-rGO/GCE in 5 mM $[Fe(CN)_6]^{3-/4-}$ solution, its parameter settings: 10, 30, 50, 70, 90, 110, 130, 150, 170, 190, 210, 230, 250, 270, 290, and 310 mV·s^{-1}. As displayed in Fig. 2C, the relevant linear regression equations were as follows, where the anode: *Ipa* (μA) = 506.173 $v^{1/2}$ − 6.815 (R^2 = 0.9999), and the cathode: *Ipc* (μA) = − 484.30$v^{1/2}$ + 4.998 (R^2 = 0.9998), indicating that the redox process on the electrode surface was a diffusion-controlled reaction. As displayed in Fig. 2D, with the increase of scanning rate, the oxidation peak potential shifted positively, and the reduction peak potential shifted negatively. When $\Delta Ep > 110$ mV, the relevant linear regression equations were as follows, where the anode: E_{pa} (V) = 0.05496 *lg* (v) + 0.30707 (R^2 = 0.981), and the cathode: E_{pc} (V) = − 0.06071 *lg* (v) + 0.08845 (R^2 = 0.981). Moreover, according to the Laviron theory [36]:

$$\lg \frac{k_a}{k_c} = \lg \frac{\alpha}{1-\alpha} \tag{2}$$

$$lgk_s\ \alpha\ lg(1-a) + (1-a)lga - lg(\frac{RT}{nFv}) - \frac{2.3RTa}{(1-a)nF \triangle k_p} \tag{3}$$

where k_a and k_c are the slopes of E_{pa} to *lg* (v) and E_{pc} to *lg* (v), respectively. *R*, *T*, and *F* are gas constant, room temperature, and Faraday constant, respectively, $n = 1$. Based on Eqs. (2) and (3), $\alpha = 0.475$ (charge transfer coefficient) and $k_s = 1.167$ s^{-1} (apparent electron transfer rate constant). The k_s was better than the reported in the article (Table S2), which indicated MoS_2-rGO enhanced the electron transfer.

Electrochemical characterization of the modified electrodes

CV was used to characterize the modification steps of electrode surface (Fig. 3A). After applying MoS_2-rGO to the GCE, the peak signal increased (curve b), which may be due

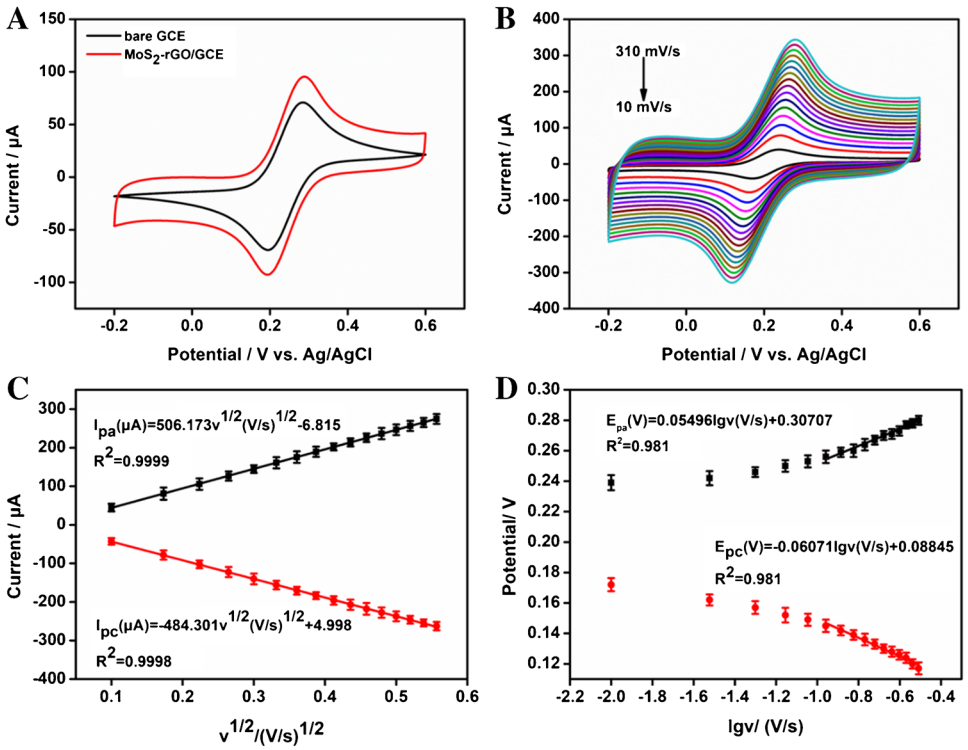

Fig. 2 **A** CV of bare GCE, MoS_2-rGO/GCE, and AuNPs/MoS_2-rGO/GCE. **B** CV curves of MoS_2-rGO/GCE at different scan rates. **C** The linear relationship between the anodic and cathodic peak currents versus scan rate. **D** The linear relationship between the anodic and cathodic peak potentials versus scan rate

to the fact that the flake rGO loading with flower-like MoS_2 could improve the conductivity of the modified electrode and accelerate the electron transfer. After AuNPs were deposited on MoS_2-rGO/GCE, the electrochemical signal (curve c) was further enhanced owing to the excellent conductivity of AuNPs. Then, the current response (curve d) dropped sharply when the capture probes (SH-CP) were loaded on AuNPs/MoS_2-rGO/GCE, which could be attributed to the steric hindrance and electrostatic repulsive force of SH-CP to $[Fe(CN)_6]^{3-/4-}$. Similarly, the current further decreased (curve e) after the MCH was fixed on the CP/AuNPs/MoS_2-rGO/GCE. As the macromolecule miRNA-21 was added to the electrode, the peak current was decreased again (curve f). The result was because that dsDNA's polymerization increased the electrostatic repulsion between potassium ferricyanide and the electrode surface. As expected, the current response reduced (curve g) when the S1-AuNPs-HRP nanoprobes were applied to the modified electrode, which could explain that the negatively charged DNA and high molecular weight proteins made the modified electrode insulated, and electron transfer became more obstructed. The results above showed that the electrode modification step by step was successful.

EIS is an important tool to investigate the assembling procedure of sensing electrode surface. As displayed in the inset in Fig. 3B, the equivalent circuit was employed to study the EIS Nyquist plots of whole assembly process. Firstly, the R_{ct} of the bare GCE was with a small semicircle (curve a, 117.6 Ω). When MoS_2-rGO was applied on the GCE, the R_{ct} value significantly decreased, which was ascribed to the excellent conductivity of the MoS_2-rGO (curve b, 35 Ω). After the AuNPs were electrodeposited on the modified electrode, the R_{ct} dropped further and exhibited almost a straight line (curve c, 0.8 Ω) due to the synergistic effect of AuNPs and supporting substrate. However, when capture probes (curve d, 72 Ω), MCH (curve e, 96 Ω), miRNA-21 (curve f, 165 Ω), and S1-AuNPs-HRP nanoprobes (curve g, 300 Ω) were stepwise modified onto the AuNPs/MoS_2-rGO/GCE, a successively increased R_{ct} could be seen. The following fact could explain the results above that macromolecular proteins and more phosphate backbone of DNA polymers were attached to the modified electrode, and hindered the transfer of electrons on the electrode surface. All the EIS results were in conformity with CV in Fig. 3A, indicating the successful construction of miRNA detection platform.

Meanwhile, to demonstrate the synergistic amplification of 3D MoS_2-rGO and AuNPs-HRP, the DPV responses of different modified electrodes were studied in 0.1 M PBS containing 2 mM HQ and 2 mM H_2O_2. As displayed in Fig. 3C, in the absence of AuNPs-HRP, the DPV signal (curve b) of S1-AuNPs/miRNA-21/MCH/CP/AuNPs/MoS_2-rGO/GCE was weak. At the same time, it could be observed that the DPV signal (curve c) of S1-AuNPs-HRP/miRNA-21/MCH/CP/AuNPs/GCE was also weak when there was no 3D MoS_2-rGO. However, when 3D MoS_2-rGO and AuNPs-HRP were used together to modify the electrode, a strong DPV signal (curve d) was generated. The above phenomenon could

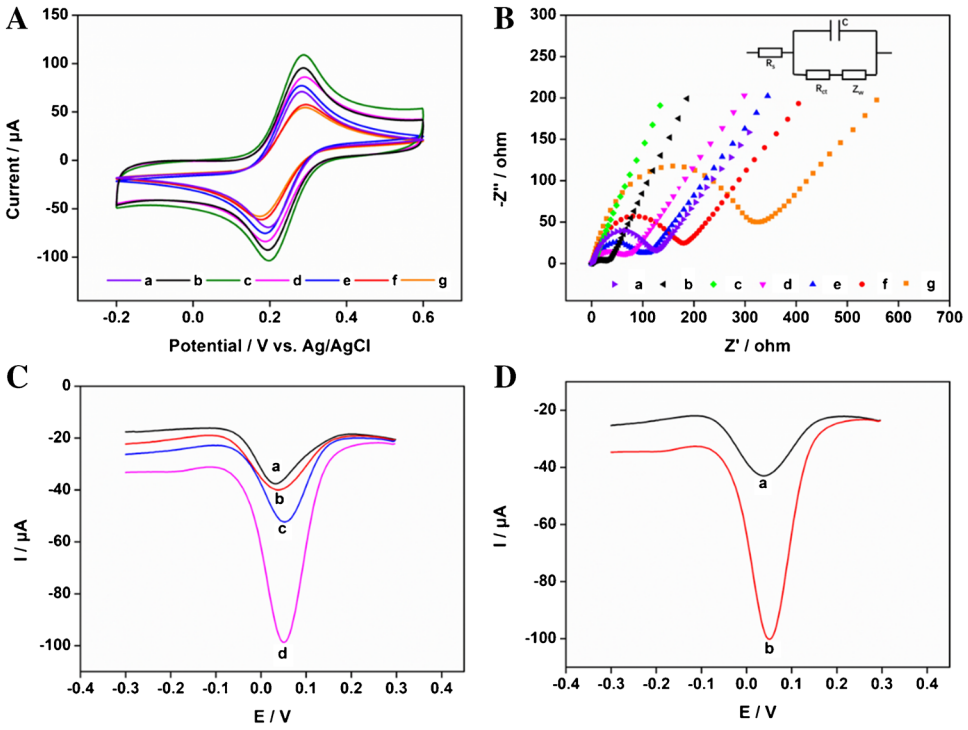

Fig. 3 **A** CV and **B** EIS of (a) bare GCE, (b) MoS_2-rGO/GCE, (c) AuNPs/MoS_2-rGO/GCE, (d) CP/AuNPs/MoS_2-rGO/GCE, (e) MCH/CP/AuNPs/MoS_2-rGO/GCE, (f) miRNA-21/MCH/CP/AuNPs/MoS_2-rGO/GCE, (g) S1-AuNPs-HRP/miRNA-21/MCH/CP/AuNPs/MoS_2-rGO/GCE; **C** DPVs of bare GCE (a), S1-AuNPs/miRNA-21/MCH/CP/AuNPs/MoS_2-rGO/GCE (b), S1-AuNPs-HRP/miRNA-21/MCH/CP/AuNPs/GCE (c), and S1-AuNPs-HRP/miRNA-21/MCH/CP/AuNPs/MoS_2-rGO/GCE (d) in 0.1 M PBS (pH 7.4) including 2 mM HQ and 2 mM H_2O_2; **D** DPVs of the modified electrodes in 0.1 M PBS (pH 7.4) including 2 mM HQ and 2 mM H_2O_2: the absence (a) or presence (b) of miRNA-21

explain that the simultaneous presence of 3D MoS_2-rGO and AuNPs-HRP could significantly enhance the current response, which played a vital role in improving the detection sensitivity.

In the presence or absence of miRNA-21, the DPV signals of the prepared electrodes are shown in Fig. 3D. When the miRNA-21 existed, an obvious electrochemical signal could be seen from curve b, which could be attributed to the fact that the presence of the target miRNA-21 made the HRP with catalysis and signal amplification integrate into the electrode. However, almost no response was emerged in curve a compared to curve b, which was attributed to the lack of HRP that could catalyze the substrate reaction in the system.

The analysis of PAGE gel electrophoresis

The results of PAGE gel electrophoresis further provided evidence for the successful hybridization of the probes and miRNA-21 (Fig. S4). The capture probes (CP), DNA strand S1 (S1), and target miRNA-21 corresponded to the bands from lane 5, lane 3, and lane 6, respectively. After incubating the miRNA-21 with the CP and the S1, respectively, shorter bands could be seen (lane 3, lane 4) due to the increment of molecular weight after pairing. Meanwhile, a conspicuous band close to 50 bp was observed (lane 2) with lower electrophoretic mobility than lane 3 and lane 4, which was attributed to the hybrid of CP, target miRNA-21, and the S1.

Optimization of the experimental conditions

The experimental conditions significantly affect the detection performances of the biosensor. Therefore, some important experimental parameters (deposition time of AuNPs, the incubation time of capture probes and miRNA-21, as well as incubation time between S1-AuNPs-HRP and the miRNA-21) were studied. The results and descriptions are shown in Electronic Supplementary Material (Fig. S5).

Electrochemical detection of miRNA-21

Under the optimized experimental conditions, the DPV was adopted to study the detection performance of the prepared biosensor. As depicted in Fig. 4A, the peak signal enhanced with the increase of miRNA-21 concentration and showed an excellent linear range from 5×10^{-1} to 5×10^{-9} μM and the linear equation was I (μA) = -5.89 lg (c/μM) -71.69 with a correlation coefficient of 0.995, the sensitivity was 67.62 μA μM^{-1} cm^{-2} and the detection limit was estimated to be 0.54 fM ($S/N=3$), where I represented the peak current and c represented the concentration of miRNA-21. Compared with other previously reported test results (Table 1), the detection performance was better than or comparable to some previous works. The satisfactory result could be attributed to the following points: (1) 3D MoS_2-rGO had a large specific surface area and excellent conductivity; (2) 3D MoS_2-rGO nanocomposites and HRP synergistically amplified the signal in H_2O_2+HQ system. These

advantages made the prepared biosensor with higher sensitivity for target miRNA detection.

Selectivity, repeatability, and stability

To evaluate the selectivity of the proposed biosensor, the DPV responses of the biosensor toward miRNA-21, five interferences (miRNA-155, miRNA let-7a, non-complementary sequence, three-base mismatched, double-base mismatched), and their mixture were investigated. As shown in Fig. S6, the DPV responses for the detection of 500 pM interfering miRNA were almost the same as that of the blank sample, while a significant increase of the DPV response was recorded with the presence of 5 pM miRNA-21. In addition, the DPV signal of the biosensor toward the mixture of miRNA-21 and interfering miRNA revealed a similar DPV response compared with that of miRNA-21, confirming that the proposed biosensor had good selectivity.

Five electrodes were made in the same way to study the repeatability of the proposed biosensor. According to the results in Fig. 5A, the relative standard deviation (RSD) was 1.6% when the proposed biosensor was used to detect 50 pM miRNA-21, respectively, indicating a satisfactory reproducibility. In addition, the stability of the modified electrodes was studied by storing the proposed miRNA biosensor at 4 °C for 20 days and the electrochemical response was recorded. According to the results in Fig. 5B, 96% of the original response was retained, which suggested that the prepared biosensor had excellent stability.

Analytical application in serum sample

To evaluate the application potential and feasibility of the prepared biosensor, the method of standard addition was adopted to analyze miRNA-21 in normal human serum samples. Various concentrations of miRNA-21 (5 pM, 50 pM, and 500 pM) were spiked into the serum samples diluted 10 times. Each sample was then analyzed with the biosensors. As shown in Table 2, the recoveries were from 97.80 to 103.54%, and the RSD values were from 2.40 to 5.86%, demonstrating that the proposed biosensor had great potentiality in monitoring miRNA-21 in real clinical analysis.

Conclusions

In summary, an ultrasensitive miRNA-21 detection platform was established by introducing the 3D MoS_2/rGO nanocomposites and AuNPs-HRP nanoprobes. The 3D MoS_2/rGO nanocomposites provided excellent electron conductivity. Besides, the use of HRP with high catalytic activity as signal molecules in H_2O_2 + HQ system could achieve efficient and reliable signal amplification. The prepared biosensor has a wider linear range from 5 fM to 0.5 μM, high sensitivity (67.62 μA μM^{-1} cm^{-2}), low detection limit (0.54 fM), excellent selectivity, and long-term storage stability, showing an outstanding electrochemical performance for miRNA-21 detection. Therefore, the

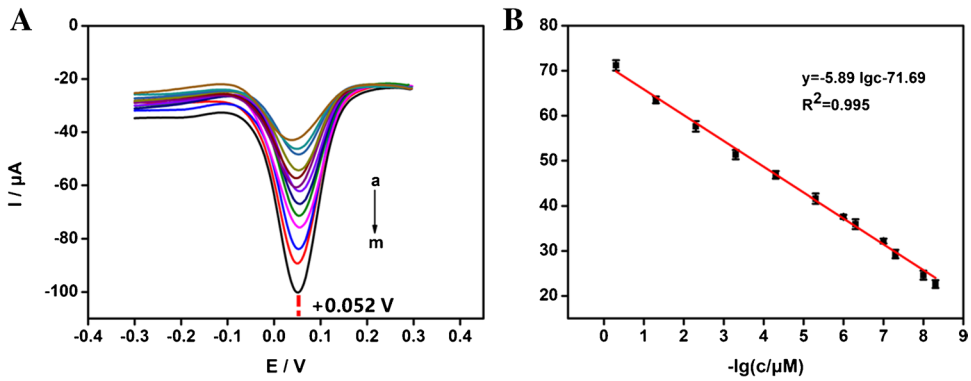

Fig. 4 **A** DPVs of different concentrations of miRNA-21 in 0.1 M PBS (pH = 7.4) (a to m): 0, 5×10^{-9}, 1×10^{-8}, 5×10^{-8}, 1×10^{-7}, 5×10^{-7}, 1×10^{-6}, 5×10^{-6}, 5×10^{-5}, 5×10^{-4}, 5×10^{-3}, 5×10^{-2}, 5×10^{-1} μM, respectively. **B** The linear relation of DPV current and the negative logarithm of target miRNA-21. Error bars: *SD*, $n = 3$

Table 1 Comparison of the proposed biosensor with other techniques for detecting miRNA

Materials	Detection modes	Linear range	Detection limit	Reference
Poly(TMSMA-r-PEGMA-r-NAS)	Electrochemistry	10 fM ~ 1 nM	2 fM	[37]
Pt/MWCNT	Electrochemistry	10 fM ~ 1 nM	1.64 fM	[7]
MoS_2-Thionine-AuNPs	Electrochemistry	1 pM ~ 10 nM	0.26 pM	[30]
Au/PPy-rGO	Electrochemistry	10 fM ~ 5 nM	1.57 fM	[3]
GO/GNR/OB	Electrochemistry	2 fM ~ 8 pM	0.6 fM	[38]
SnO_2/$CdCO_3$/CdS	Photoelectrochemical	10 fM ~ 1 μM	3.25 fM	[39]
AuNP-PNT	Electrochemistry	10 fM ~ 0.3 nM	3.90 fM	[40]
Pt/Sn–In_2O_3 nanoflower	Electrochemistry	5 pM ~ 5 fM	1.92 fM	[41]
SWCNTs	Electrochemistry	10 fM ~ 0.3 nM	3.5 fM	[42]
3D MoS_2-rGO; HRP	Electrochemistry	5 fM ~ 0.5 μM	0.54 fM	This work

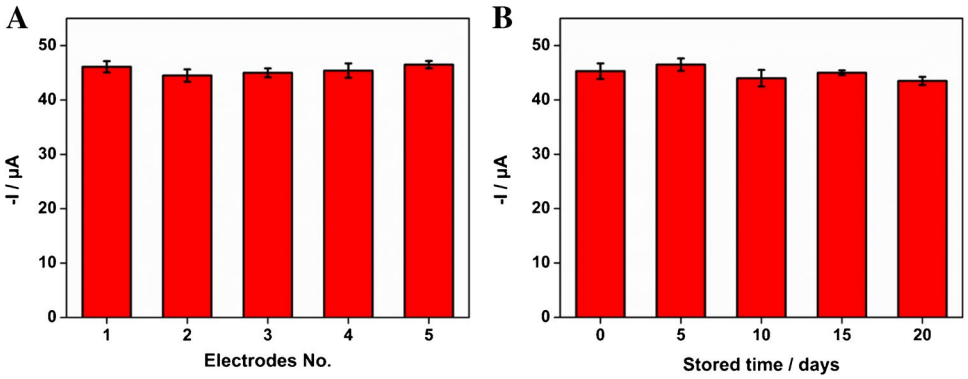

Fig. 5 **A** The current response of five repetitive experiments. **B** The storage stability of the miRNA biosensor in a refrigerator (4 °C). The concentration of miRNA-21 was 50 pM. Error bars: *SD*, $n = 3$

Table 2 Determination of miRNA-21 added in normal human serum with the proposed biosensor ($n = 3$). The normal human serum was diluted tenfold by 0.01 M PBS

Sample	Add (pM)	Found (pM)	Recovery (%)	RSD (%)
1	0	/	/	/
2	5	4.89 pM	97.80	2.40
3	50	50.40 pM	100.80	5.86
4	500	517.70 pM	103.54	1.21

constructed platform offers an efficient protocol for sensitive determination of miRNA, which has great potential in the early diagnosis of clinical diseases and the bioassay of other related subjects.

Supplementary Information The online version contains supplementary material available at https://doi.org/10.1007/s00604-021-05141-0.

Funding This work was supported by the National Natural Science Foundation of China (NO. 81772290), Graduate Scientific Research and Innovation Foundation of Chongqing, China (CYS21069, 2020CDCGJ014), Fundamental Research Funds for the Central Universities (2021CDJYGRH006), National Facility for Translational Medicine (Shanghai) Open Research Fund (TMSK-2021–113), Science and Technology Research Program of Chongqing Education Commission of China (KJCXZD2020008), Chongqing Graduate Tutor Team Construction Project, Analytical and Testing Center of Chongqing University for (FE-SEM / XPS / XRD) and the sharing fund of Chongqing University's large equipment.

Declarations

Conflict of interest The authors declare no competing interests.

References

1. Guo W-J, Wu Z, Yang X-Y, Pang D-W, Zhang Z-L (2019) Ultrasensitive electrochemical detection of microRNA-21 with wide linear dynamic range based on dual signal amplification. Biosens Bioelectron 131:267–273
2. Kangkamano T, Numnuam A, Limbut W, Kanatharana P, Vilaivan T, Thavarungkul P (2018) Pyrrolidinyl PNA polypyrrole/silver nanofoam electrode as a novel label-free electrochemical miRNA-21 biosensor. Biosens Bioelectron 102:217–225
3. Bao J, Hou C, Zhao Y, Geng X, Samalo M, Yang H, Bian M, Huo D (2019) An enzyme-free sensitive electrochemical microRNA-16 biosensor by applying a multiple signal amplification strategy based on Au/PPy–rGO nanocomposite as a substrate. Talanta 196:329–336
4. D.D. Cao, L. Li, W.Y. Chan (2016) MicroRNAs: key regulators in the central nervous system and their implication in neurological diseases. Intern J Mol Sci 17(6)
5. Asif M, Aziz A, Ashraf G, Wang Z, Wang J, Azeem M, Chen X, Xiao F, Liu H (2018) Facet-inspired core–shell gold nanoislands on metal oxide octadecahedral heterostructures: high sensing performance toward sulfide in biotic fluids. ACS Appl Mater Interfaces 10(43):36675–36685
6. C. Zhou, K. Cui, Y. Liu, L. Li, L. Zhang, M. Xu, S. Ge, Y. Wang, J. Yu (2020) Ultrasensitive lab-on-paper device via Cu/Co double-doped CeO2 nanospheres as signal amplifiers for electrochemical/visual sensing of miRNA-155. Sens Act B: Chem 321 128499
7. Cai W, Xie S, Tang Y, Chai Y, Yuan R, Zhang J (2017) A label-free electrochemical biosensor for microRNA detection based on catalytic hairpin assembly and in situ formation of molybdophosphate. Talanta 163:65–71
8. G.S. Pall, C. Codony-Servat, J. Byrne, L. Ritchie, A. Hamilton (2007) Carbodiimide-mediated cross-linking of RNA to nylon membranes improves the detection of siRNA, miRNA and piRNA by northern blot. Nuc Acids Res 35(8)
9. Asif M, Aziz A, Wang Z, Ashraf G, Wang J, Luo H, Chen X, Xiao F, Liu H (2019) Hierarchical CNTs@CuMn layered double hydroxide nanohybrid with enhanced electrochemical performance in H2S detection from live cells. Anal Chem 91(6):3912–3920
10. Asif M, Haitao W, Shuang D, Aziz A, Zhang G, Xiao F, Liu H (2017) Metal oxide intercalated layered double hydroxide nanosphere: with enhanced electrocatalyic activity towards H2O2 for biological applications. Sens Actuators, B Chem 239:243–252
11. Miao P, Zhang T, Xu J, Tang Y (2018) Electrochemical detection of miRNA combining T7 exonuclease-assisted cascade signal amplification and DNA-templated copper nanoparticles. Anal Chem 90(18):11154–11160
12. Jeong K, Yu YJ, You JY, Rhee WJ, Kim JA (2020) Exosome-mediated microRNA-497 delivery for anti-cancer therapy in a microfluidic 3D lung cancer model. Lab Chip 20(3):548–557
13. Aziz A, Asif M, Azeem M, Ashraf G, Wang Z, Xiao F, Liu H (2019) Self-stacking of exfoliated charged nanosheets of LDHs and graphene as biosensor with real-time tracking of dopamine from live cells. Anal Chim Acta 1047:197–207
14. Asif M, Liu H, Aziz A, Wang H, Wang Z, Ajmal M, Xiao F, Liu H (2017) Core-shell iron oxide-layered double hydroxide: high electrochemical sensing performance of H2O2 biomarker in

live cancer cells with plasma therapeutics. Biosens Bioelectron 97:352–359
15. M. Asif, A. Aziz, G. Ashraf, T. Iftikhar, Y. Sun, F. Xiao, H. Liu (2022) Unveiling microbiologically influenced corrosion engineering to transfigure damages into benefits: a textile sensor for H2O2 detection in clinical cancer tissues. Chem Engin J 427 131398
16. A. Aziz, M. Asif, G. Ashraf, T. Iftikhar, J. Hu, F. Xiao, S. Wang (2022) Boosting electrocatalytic activity of carbon fiber@fusiform-like copper-nickel LDHs: sensing of nitrate as biomarker for NOB detection. J Hazard Mat 422 126907
17. Huang KJ, Shuai HL, Zhang JZ (2016) Ultrasensitive sensing platform for platelet-derived growth factor BB detection based on layered molybdenum selenide-graphene composites and exonuclease III assisted signal amplification. Biosens Bioelectron 77:69–75
18. K.R. Reddy, B. Hemavathi, G.R. Balakrishna, A.V. Raghu, S. Naveen, M.V. Shankar, 11 - Organic conjugated polymer-based functional nanohybrids: synthesis methods, mechanisms and its applications in electrochemical energy storage supercapacitors and solar cells, in: K. Pielichowski, T.M. Majka (Eds.), Polymer composites with functionalized nanoparticles, Elsevier2019, pp. 357–379
19. Asif M, Aziz A, Wang H, Wang Z, Wang W, Ajmal M, Xiao F, Chen X, Liu H (2019) Superlattice stacking by hybridizing layered double hydroxide nanosheets with layers of reduced graphene oxide for electrochemical simultaneous determination of dopamine, uric acid and ascorbic acid. Microchim Acta 186(2):61
20. Kumar S, Reddy KR, Reddy CV, Shetti NP, Sadhu V, Shankar MV, Reddy VG, Raghu AV, Aminabhavi TM (2021) Metal nitrides and graphitic carbon nitrides as novel photocatalysts for hydrogen production and environmental remediation. In: Balakumar S, Keller V, Shankar MV (eds) Nanostructured materials for environmental applications. Springer International Publishing, Cham, pp 485–519
21. Lukowski MA, Daniel AS, Meng F, Forticaux A, Li L, Jin S (2013) Enhanced hydrogen evolution catalysis from chemically exfoliated metallic MoS2 nanosheets. J Am Chem Soc 135(28):10274–10277
22. Wang Y, Wang Y, Wu D, Ma H, Zhang Y, Fan D, Pang X, Du B, Wei Q (2018) Label-free electrochemical immunosensor based on flower-like Ag/MoS2/rGO nanocomposites for ultrasensitive detection of carcinoembryonic antigen. Sens Actuators, B Chem 255:125–132
23. Zhou S, Gao J, Wang S, Fan H, Huang J, Liu Y (2020) Highly efficient removal of Cr(VI) from water based on graphene oxide incorporated flower-like MoS2 nanocomposite prepared in situ hydrothermal synthesis. Environ Sci Pollut Res 27(12):13882–13894
24. T. Mathew, R.A. Sree, S. Aishwarya, K. Kounaina, A.G. Patil, P. Satapathy, S.P. Hudeda, S.S. More, K. Muthucheliyan, T.N. Kumar, A.V. Raghu, K.R. Reddy, F. Zameer (2020) Graphene-based functional nanomaterials for biomedical and bioanalysis applications. FlatChem 23 100184
25. Hodala JL, Moon DJ, Reddy KR, Reddy CV, Kumar TN, Ahamed MI, Raghu AV (2021) Catalyst design for maximizing C5+ yields during Fischer-Tropsch synthesis. Int J Hydrogen Energy 46(4):3289–3301
26. K. Kannan, D. Radhika, A.S. Nesaraj, K. Kumar Sadasivuni, K.R. Reddy, D. Kasai, A.V. Raghu (2020) Photocatalytic, antibacterial and electrochemical properties of novel rare earth metal oxides-based nanohybrids. Mat Sci Energy Technol 3 853–861
27. Song S, Qin Y, He Y, Huang Q, Fan C, Chen HY (2010) Functional nanoprobes for ultrasensitive detection of biomolecules. Chem Soc Rev 39(11):4234–4243
28. Chen Z, Lai G, Liu S, Yu A (2018) Ultrasensitive electrochemical aptasensing of kanamycin antibiotic by enzymatic signal amplification with a horseradish peroxidase-functionalized gold nanoprobe. Sens Actuators, B Chem 273:1762–1767
29. Liu F, Xiang G, Jiang D, Zhang L, Chen X, Liu L, Luo F, Li Y, Liu C, Pu X (2015) Ultrasensitive strategy based on PtPd nanodendrite/nano-flower-like@GO signal amplification for the detection of long non-coding RNA. Biosens Bioelectron 74:214–221
30. Zhu D, Liu W, Zhao D, Hao Q, Li J, Huang J, Shi J, Chao J, Su S, Wang L (2017) Label-free electrochemical sensing platform for MicroRNA-21 detection using thionine and gold nanoparticles co-functionalized MoS2 nanosheet. ACS Appl Mater Interfaces 9(41):35597–35603
31. Cheng F-F, He T-T, Miao H-T, Shi J-J, Jiang L-P, Zhu J-J (2015) Electron transfer mediated electrochemical biosensor for microRNAs detection based on metal ion functionalized titanium phosphate nanospheres at attomole level. ACS Appl Mater Interfaces 7(4):2979–2985
32. Z. Liang, D. Ou, D. Sun, Y. Tong, H. Luo, Z. Chen (2019) Ultrasensitive biosensor for microRNA-155 using synergistically catalytic nanoprobe coupled with improved cascade strand displacement reaction. Bios Bioel 146 111744
33. Li F, Zhang L, Li J, Lin X, Li X, Fang Y, Huang J, Li W, Tian M, Jin J, Li R (2015) Synthesis of Cu-MoS2/rGO hybrid as non-noble metal electrocatalysts for the hydrogen evolution reaction. J Power Sources 292:15–22
34. Dai G, Li Z, Luo F, Ai S, Chen B, Wang Q (2019) Electrochemical determination of Salmonella typhimurium by using aptamer-loaded gold nanoparticles and a composite prepared from a metal-organic framework (type UiO-67) and graphene. Microchim Acta 186(9):620
35. X. Hou, Z. Wang, G. Fan, H. Ji, S. Yi, T. Li, Y. Wang, Z. Zhang, L. Yuan, R. Zhang, J. Sun, D. Chen (2020) Hierarchical three-dimensional MoS2/GO hybrid nanostructures for triethylamine-sensing applications with high sensitivity and selectivity. Sensors and Actuators, B: Chemical 317
36. Yin H, Ma Q, Zhou Y, Ai S, Zhu L (2010) Electrochemical behavior and voltammetric determination of 4-aminophenol based on graphene-chitosan composite film modified glassy carbon electrode. Electrochim Acta 55(23):7102–7108
37. Fang CS, Kim KS, Yu B, Jon S, Kim MS, Yang H (2017) Ultrasensitive electrochemical detection of miRNA-21 using a zinc finger protein specific to DNA-RNA hybrids. Anal Chem 89(3):2024–2031
38. Azimzadeh M, Rahaie M, Nasirizadeh N, Ashtari K, Naderi-Manesh H (2016) An electrochemical nanobiosensor for plasma miRNA-155, based on graphene oxide and gold nanorod, for early detection of breast cancer. Biosens Bioelectron 77:99–106
39. Y.X. Wen, M. Qing, S.L. Chen, H.Q. Luo, N.B. Li (2021) Y-type DNA structure stabilized p-type CuS quantum dots to quench photocurrent of ternary heterostructure for sensitive photoelectrochemical detection of miRNA. Sensors and Actuators, B: Chemical 329
40. Y.T. Yaman, O.A. Vural, G. Bolat, S. Abaci (2020) One-pot synthesized gold nanoparticle-peptide nanotube modified disposable sensor for impedimetric recognition of miRNA 410. Sensors and Actuators, B: Chemical 320
41. Zhang K, Dong H, Dai W, Meng X, Lu H, Wu T, Zhang X (2017) Fabricating Pt/Sn-In2O3 nanoflower with advanced oxygen reduction reaction performance for high-sensitivity microRNA electrochemical detection. Anal Chem 89(1):648–655
42. Chen Z, Xie Y, Huang W, Qin C, Yu A, Lai G (2019) Exonuclease-assisted target recycling for ultrasensitive electrochemical detection of microRNA at vertically aligned carbon nanotubes. Nanoscale 11(23):11262–11269